Synthesis, Structure, and Magnetic Properties of *catena*-(μ-Oxo)(hemiporphyrazinato)iron(IV), the First Polymeric μ-Oxo-Bridged Complex of Iron

Wolfgang Hiller,[1a] Joachim Strähle,[1a] Armin Datz,[1b] Michael Hanack,[1b] William E. Hatfield,*[1c] Leonard W. ter Haar,[1c] and Philipp Gütlich[1d]

Contribution from the Institut für Anorganische Chemie der Universität Tübingen, the Institut für Organische Chemie der Universität Tübingen, the Institut für Anorganische und Analytische Chemie der Johannes Gutenberg-Universität, Mainz, West Germany, and the Department of Chemistry, The University of North Carolina at Chapel Hill, Chapel Hill, North Carolina 27514. *Received April 11, 1983*

Abstract: The crystal and molecular structure of the compound *catena*-(μ-oxo)(hemiporphyrazinato)iron(IV), $[FeON_8C_{26}H_{14}]_n$, has been determined from single-crystal, three-dimensional X-ray diffraction counter data. The compound crystallizes as blue-black needles in space group $P2/n$ with $Z = 2$ and unit cell dimensions (at 210 K) $a = 16.090$ (3) Å, $b = 3.975$ (2) Å, $c = 16.070$ (3) Å, and $\beta = 92.97$ (1)°. The structure was refined by full-matrix least-squares techniques to a conventional R value of 0.045. Distorted (hemiporphyrazinato)iron units stack along the b axis and are linked into polymeric, uniformly spaced, linear chains by axially bound oxygen bridges. The oxygen atoms are disordered into two crystallographically distinct sites lying about a central location which is normal to the C_2 axis collinear with the chain. The Fe–O–Fe angles are 158.2° and 170.5°, and the Fe–O bond distances range from 1.973 to 2.030 Å. Mössbauer spectral studies at 4.2 K, room temperature, and 420 K reveal that there are two iron sites in the chain as a result of the disorder of the oxygen atoms, and the spectrum is essentially temperature independent. Magnetic susceptibility studies reveal that the iron ions are antiferromagnetically coupled in an alternating chain with $J = -133$ cm^{-1}, $g = 2.3$, and an alternation parameter of 0.4.

In the last few years there has been great interest in the polymeric (μ-oxo)phthalocyaninato complexes of silicon and germanium, since after being doped with iodine, the partially oxidized compounds exhibit high electrical conductivities (up to 10 Ω^{-1} cm^{-1}).[2] Corresponding complexes with the transition metals titanium and vanadium are monomers with terminal oxo ligands that exhibit strong π-bonds to the central atom.[3] (Tetraphenylporphinato)iron forms μ-oxo-bridged, dimeric complexes, $[(TPP)Fe]_2O$ (H_2TPP = tetraphenylporphyrin).[4] An analogous dimeric μ-nitrido complex has also been reported in which the formal oxidation state of the iron is +3.5.[5] It has been shown by cyclic voltammetric studies that [Fe(TPP)]Cl and $[Fe(TPP)]_2O$ easily undergo reversible one-electron oxidations to Fe(IV) or Fe(III,IV). An oxidation state of +IV for iron has recently been proposed for the (tetraphenylporphyrinato)iron complex [Fe(O)(TPP)(1-meim)][6] (meim = 1-methylimidazole). We report here the synthesis, structure, and properties of $[FeOHp]_n$ (where H_2Hp = hemiporphyrazine), the first polymeric μ-oxo-bridged complex of iron. On the basis of chemical and physical properties we assign a formal oxidation state of +IV and spin value $S = 1$ to the iron atom in this novel complex.

Experimental Section

Preparation and Characterization. Polymeric (μ-oxo)(hemiporphyrazinato)iron, $[FeOHp]_n$, is prepared by treating hemiporphyrazine (H_2Hp) with iron(II) acetate in boiling nitrobenzene over a period of 30 min. Under these conditions nitrobenzene acts as an oxidizing agent, since $[FeOHp]_n$ is also obtained when the reaction is carried out in an inert atmosphere. Black, needlelike single crystals were formed on recrystallization of the curde product from nitrobenzene by slow cooling of the solution. The crystals were washed with methanol.

A solution of (hemiporphyrazinato)bis(pyridine)iron(II), $[HpFe(py)_2]$,[7] in pyridine is easily oxidized in air to $[FeOHp]_n$. The polymer $[FeOHp]_n$ is quite stable in bases (KOH, pyridine) but decomposes in the presence of strong acids with loss of the metal. There is a weight loss in the thermogravimetric analysis between 630 and 650 K that corresponds to the expected weight loss of an oxygen atom per FeHp unit. The ion of highest mass in the mass spectrum is $FeOHp^+$ (m/e 510). The infrared spectrum of $[FeOHp]_n$ differs from that of [FeHp][7] (which has been prepared in pure form for the first time) principally in the region between 700 and 900 cm^{-1} ([FeHp]: 770 w, 810 m, 890 w; $[FeOHp]_n$: 732 s, 773 s, 801 w, 810 m, 821 s, 895 vs).

Mössbauer effect spectra were recorded with a constant-acceleration Mössbauer spectrometer equipped with a custom-built furnace and a liquid helium cryostat, and the fittings of sums of Lorentzian lines to the measured spectra were carried out by use of a least-squares iteration computer program.

Magnetic susceptibility data were collected in Mainz by using a Foner-type vibrating sample magnetometer over the temperature range 3.35–294.8 K and in Tübingen by using a Gouy balance[9] over the temperature range 113.2–423 K. The data sets were in good agreement. The vibrating sample magnetometer was operated at 10 kOe for the measurements and was calibrated with $HgCo(NCS)_4$,[8] while the magnetic equipment in Tübingen was calibrated with $NiCl_2$.[9] Diamagnetic corrections for the constituent atoms were made by using Pascal's constants.[10] A flow-type cryostat with an internal helium reservoir was used, and the temperatures were measured with a calibrated Au(0.3% Fe)/chromel thermocouple.

Although the compound is paramagnetic, attempts to record an EPR spectrum with a Varian E-112 spectrometer at several temperatures (292, 113, 80 K) were unsuccessful.

Crystallographic Data and Structure Determination. The compound $[FeOHp]_n$ crystallizes as blue-black needles. A single crystal with the approximate dimensions 0.15 × 0.15 × 0.9 mm^3 was chosen for the X-ray investigation. A monoclinic space group $P2/n$ was established on the basis of Buerger precession photographs. The lattice constants were determined accurately by using an automatic single-crystal diffractom-

(1) (a) Institut für Anorganische Chemie der Universität Tübingen. (b) Institut für Organische Chemie der Universität Tübingen. (c) The University of North Carolina at Chapel Hill. (d) Institut für Anorganische und Analytische Chemie der Johannes Gutenberg-Universität.

(2) (a) Dirk, C. W.; Mintz, E. A.; Schoch, K. F., Jr.; Marks, T. J. *Sci. Chem.* **1981**, *16*, 275. (b) Marks, T. J.; Schoch, K. F., Jr.; Kundalkar, B. R. *Synth. Met.* **1980**, *1*, 337. (c) Schoch, K. F., Jr.; Kundalkar, B. R.; Marks, T. J. *J. Am. Chem. Soc.* **1979**, *101*, 7071. (d) Diel, B. M.; Inabe, T.; Lyding, J. W.; Schoch, K. F., Jr.; Kannewurf, C. R.; Marks, T. J. *Polym. Prepr., Am. Chem. Soc., Div. Polym. Chem.* **1982**, *23*, 124. (e) Metz, J.; Pawlowski, G.; Hanack, M. *Z. Naturforsch., B*, in press.

(3) Hiller, W.; Strähle, J.; Kobel, W.; Hanack, M. *Z. Kristallogr.* **1982**, *159*, 173.

(4) Hoffman, A. B.; Collins, D. M.; Day, V. W.; Fleischer, E. B.; Srivastava, T. S.; Hoard, J. L. *J. Am. Chem. Soc.* **1972**, *94*, 3620.

(5) Kadish, K. M.; Rhodes, R. K.; Bottomley, L. A.; Goff, H. M. *Inorg. Chem.* **1981**, *20*, 3195.

(6) Simonneaux, G.; Scholz, W. F.; Reed, C. A.; Lang, G. *Biochim. Biophys. Acta* **1982**, *716*, 1.

(7) Hanack, M.; Datz, A., unpublished observations.

(8) Brown, D. B.; Crawford, V. H.; Hall, J. W.; Hatfield, W. E. *J. Phys. Chem.* **1977**, *81*, 1303–1306.

(9) Babel, D.; Greifeneder, D. *Chem.-Ing.-Tech.* **1967**, *39*, 812.

(10) Weller, R. R.; Hatfield, W. E. *J. Chem. Educ.* **1979**, *56*, 652.

0002-7863/84/1506-0329$01.50/0

Table I. Crystal Data and Data Collection Summary for $[FeOHp]_n$

molecular formula	$FeON_8C_{26}H_{14}$
mol wt	510.3
crystal class	monoclinic
space group	$P2/n$
lattice constants	
a,[a] Å	16.090 (3), 16.149 (1)
b,[a] Å	3.975 (2), 3.992 (1)
c,[a] Å	16.070 (3), 16.143 (1)
β,[a] deg	92.97 (1), 92.94 (1)
cell vol,[a] Å^3	1026.4, 1039.2
ρ_x,[a] g cm^{-3}	1.651, 1.631
crystal dimensions, mm^3	0.15 × 0.15 × 0.9
radiation	Mo Kα
μ, cm^{-1}	7.723
$2\theta_{max}$, deg	30
scan type	ω/θ
scan speed, deg min^{-1}	variable
bgd counting, deg offset	variable
final no. of parameters	167
formula units	$Z = 2$
obsd reflections	1459 with $I \geq 3\sigma(I)$
R	0.045

[a] The first value listed was obtained at 210 K and the second at 293 K.

eter, CAD4 (Enraf-Nonius, Delft), and 25 precisely centered high-angle reflections., Crystal data and data collection details are given in Table I. Two data sets were collected, one at room temperature and one at 210 K. The CAD4 was operated in the needle mode. For the structure determination 9092 intensities were measured, with an ω/θ scan from θ = 3–30° at a temperature of 210 K. After averaging over the equivalent reflections of the reciprocal lattice, there remained 1459 reflections with intensities $I > 3\sigma(I)$. Intensity data were corrected for Lorentz and polarization effects and absorption.[11]

Solution and Refinement of the Structure. The positions of the iron and nitrogen atoms N1 and N3 were deduced from a Patterson synthesis. When these positions were coupled with a difference Fourier synthesis, the missing nitrogen and carbon atoms were then located. Refinement of the positions of the iron, nitrogen, and carbon atoms with isotropic temperature factors led to an R value of 0.158.[12,13] The quantity minimized during refinement was $\sum w(|F_o| - |F_c|)^2$, where $w = 1/\sigma^2(F_o)$. The position of the bridging oxygen atom could not be determined from the data set that had been collected at room temperature. The second data set, which was collected at 210 K, allowed us to localize this position at (0.25, 0.6973, 0.25) from a difference Fourier synthesis. Upon inclusion of the anisotropic temperature parameters the reliability factor was improved to 0.072, whereupon a strong excursion of the oxygen's electron density vertical to the C_2 axis became apparent. When it was assumed that the oxygen was disordered in one site (two symmetry-related positions) the reliability factor was 0.060. However, when it was assumed that the oxygen atom was disordered in two sites, that is, four positions which lie normal to the C_2 axis, the R value was significantly improved to R = 0.054. A final difference Fourier analysis then showed no residual electron density at the original position. Incorporation of the calculated H atom positions in the structure factor calculations led to a final R value of 0.045.

Positional and thermal parameters for the atoms are given in Table II, and bond angles and bond distances are given in Table III. A table of structure factors is available as supplementary material.

Results

Description of the Structure. The crystal structure is determined by the voluminous FeHp structural units shown in Figure 1. As shown in Figure 2, the FeHp moieties are stacked up along the b axis in translationally identical units, and these are linked together with axially bound oxygen bridges to form a polymeric, linear chain with the iron atoms lying on the C_2 axes of the space group $P2/n$. The local C_2 symmetry is only fulfilled because of the disorder of the oxygen atoms, and the actual molecular symmetry around a given iron is slightly distorted. Neighboring polymer chains are arranged antiparallel to each other (see Figure 2). There is a strong distortion of the FeHp units such that the isoindole units are twisted at angles of about 30° above the mean plane, and the pyridine rings are twisted about the same amount below that plane. The twisting probably arises from the space requirements of the central iron atom. This behavior is in sharp contrast to the planar GeHp unit in $[HpGe\{C{\equiv}CC(CH_3)_3\}_2]$.[14]

The bridging oxygen atom is disordered into two crystallographically different sites (four sites overall due to the C_2 symmetry). Corresponding distances and angles are, therefore, subject

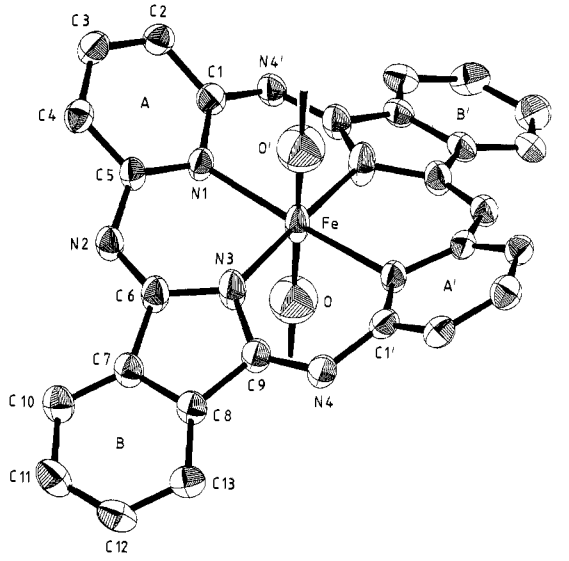

Figure 1. View of the structural unit [FeOHp] with the atom numbering scheme and labeling of the rings. The temperature factor of the oxygen atom is reduced to 50% for clarity.

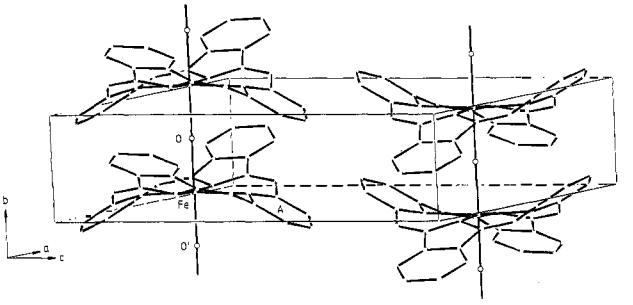

Figure 2. View of the chain structure showing the antiparallel arrangement of adjacent chains of $[FeOHp]_n$.

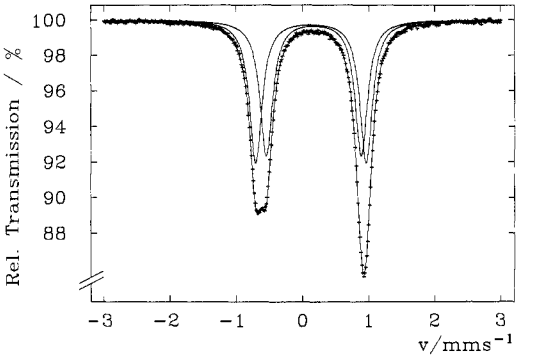

Figure 3. Mössbauer spectrum of $[FeOHp]_n$ at room temperature. Calculated lines (two quadrupole doublets) arising from two iron sites are shown along with the experimental spectrum.

(11) North, A. C. T.; Phillips, D. C.; Mathews, F. S. *Acta Crystallogr., Sect. A* **1968**, *24*, 351.

(12) Structure Determination Package (SDP), B. A. Frenz and Associates, Inc., College Station, TX, and Enraf-Nonius, Delft, Holland.

(13) Scattering factors and anomalous dispersion corrections were taken from: "International Tables for X-Ray Crystallography"; Kynoch Press: Birmingham, England, 1974; Vol. IV.

(14) Hiller, W.; Strähle, J.; Hanack, M.; Mitulla, K. *Liebigs Ann. Chem.* **1980**, 1946.

Table II

A. Atomic Positional Parameters and Isotropic Thermal Parameters (Å²) for $[FeOHp]_n$

atom	*x*	*y*	*z*	*B*	atom	*x*	*y*	*z*	*B*
Fe	0.2500	0.1943 (5)	0.2500	3.33 (3)	C7	0.0102 (3)	0.4241 (15)	0.3096 (3)	2.6 (1)
O	0.2500	0.6973 (25)	0.2500	11.9 (4)	C8	0.0015 (3)	0.4337 (15)	0.2238 (3)	2.6 (1)
O_a[a]	0.270 (1)	0.696 (6)	0.264 (2)	3.7 (5)[b]	C9	0.0775 (3)	0.2918 (15)	0.1914 (3)	2.9 (1)
O_b[a]	0.244 (1)	0.700 (4)	0.258 (3)	3.4 (5)[b]	C10	−0.0516 (3)	0.5368 (15)	0.3588 (4)	2.9 (1)
N1	0.2655 (2)[c]	0.1713 (10)	0.3826 (2)	2.53 (9)	C11	−0.1230 (3)	0.6659 (15)	0.3181 (4)	3.5 (1)
N2	0.1194 (2)	0.2160 (10)	0.4057 (2)	2.7 (1)	C12	−0.1315 (3)	0.6825 (15)	0.2320 (4)	3.2 (1)
N3	0.1320 (2)	0.2135 (15)	0.2575 (3)	3.9 (1)	C13	−0.0689 (3)	0.5672 (16)	0.1827 (4)	2.7 (1)
N4	0.0857 (2)	0.2381 (16)	0.1135 (2)	2.7 (1)	H2	0.4079	−0.0964	0.5186	5.0
C1	0.3426 (3)	0.1121 (15)	0.4190 (3)	2.3 (1)	H3	0.2911	−0.2879	0.5846	5.0
C2	0.3536 (3)	−0.0553 (15)	0.4948 (3)	2.6 (1)	H4	0.1589	−0.1349	0.5316	5.0
C3	0.2848 (3)	−0.1576 (15)	0.5349 (3)	2.9 (1)	H10	−0.0457	0.5275	0.4179	5.0
C4	0.2068 (3)	−0.0752 (15)	0.5028 (3)	2.5 (1)	H11	−0.1672	0.7422	0.3502	5.0
C5	0.1988 (3)	0.0993 (15)	0.4276 (3)	2.2 (1)	H12	−0.1808	0.7749	0.2063	5.0
C6	0.0932 (3)	0.2758 (15)	0.3305 (3)	3.0 (1)	H13	−0.0742	0.5810	0.1237	5.0

B. Anisotropic Thermal Parameters B_{ij} (10 Å²) for $[FeOHp]_n$[d]

atom	B_{11}	B_{22}	B_{33}	B_{12}	B_{13}	B_{23}	atom	B_{11}	B_{22}	B_{33}	B_{12}	B_{13}	B_{23}
Fe	14.9 (3)	69.2 (9)	16.0 (3)	0.0	1.0 (3)	1.0 (3)	C5	22 (2)	25 (3)	19 (2)	−1 (2)	3 (1)	−4 (2)
O	162 (9)	45 (6)	151 (9)	0.0	13 (8)	0.0	C6	20 (2)	49 (4)	22 (2)	−3 (2)	3 (1)	0 (2)
N1	20 (1)	40 (3)	17 (1)	−2 (2)	1 (1)	0 (2)	C7	17 (2)	33 (3)	28 (2)	−4 (2)	3 (1)	0 (2)
N2	19 (1)	39 (3)	23 (1)	−2 (2)	3 (1)	−1 (2)	C8	17 (2)	35 (3)	25 (2)	−4 (2)	0 (1)	0 (2)
N3	17 (1)	82 (4)	20 (1)	5 (2)	1 (1)	2 (2)	C9	18 (1)	47 (4)	22 (2)	−1 (2)	0 (1)	3 (2)
N4	19 (1)	39 (3)	22 (1)	−2 (2)	0 (1)	2 (2)	C10	22 (2)	35 (3)	31 (2)	−7 (2)	4 (2)	−3 (2)
C1	23 (2)	26 (3)	21 (2)	1 (2)	−1 (1)	−4 (2)	C11	23 (2)	43 (4)	39 (2)	3 (2)	2 (2)	−10 (3)
C2	28 (2)	27 (3)	22 (2)	2 (2)	−2 (2)	−1 (2)	C12	26 (2)	28 (3)	40 (2)	5 (2)	−5 (2)	−7 (3)
C3	32 (2)	31 (3)	23 (2)	0 (2)	0 (2)	4 (2)	C13	23 (2)	25 (3)	32 (2)	−3 (2)	−3 (2)	1 (2)
C4	29 (2)	26 (3)	22 (2)	−2 (2)	3 (2)	−2 (2)							

[a] Split positions. [b] Refined isotropically. Anisotropically refined atoms are given in the form of the isotropic equivalent thermal parameter defined as $(4/3)[B_{11}a^{*2} + B_{22}b^{*2} + B_{33}c^{*2} + B_{12}a^*b^* \cos\gamma + B_{13}a^*c^* \cos\beta + B_{23}b^*c^* \cos\alpha]$. [c] Estimated standard deviations for the least significant figure are in parentheses. Parameters with no standard deviations were fixed by symmetry. Hydrogen atoms were introduced in calculated positions, fixed each 0.95 Å from the appropriate carbon atom. [d] The form of the anisotropic thermal parameter is $\exp[-(1/4)(B_{11}h^2a^{*2} + \ldots + 2B_{12}hka^*b^* + \ldots)]$.

to considerable error. The Fe–O_a and Fe–O_b bond distances range from 1.973 to 2.030 Å, respectively, and are identical within the limits of error of the measurements. These distances are compatible with single covalent bonds. The Fe–O–Fe bond angles are 158.2° and 170.5° for the two different oxygen bridge types and cannot be considered identical within error limits. This will be shown below to be an important factor in the determination of the magnetic properties.

Mössbauer Spectral Studies. The Mössbauer spectrum of $[FeOHp]_n$ at room temperature is shown in Figure 3, and the isomer shift and quadrupole splitting data are given in Table IV. The identification of two distinct iron sites was unexpected in view of the results of the X-ray structural determination, which shows that the iron ions are translationally equivalent. Mössbauer spectra were collected at 420 K, room temperature, and 4.2 K, yet there were only slight variations in the isomer shift and quadrupole splitting as shown by the data in Table IV. These observations suggest that two *predominant* iron sites arise from the disorder in the oxygen sites *and* that these two iron sites exist over the entire temperature range 4.2–420 K. These data also indicate that the two different oxygen bridge types are randomly disordered and occur throughout the entire temperature range. The oxygen sites are not averaged on the Mössbauer time scale. At temperatures above 420 K, the sample begins to decompose and the Mössbauer spectra deteriorate in quality.

The increase of the isomer shift by ca. 0.2 mm s^{-1} with decreasing temperature from 420 to 4.2 K appears to be entirely due to the temperature dependence of the second-order Doppler shift; there is no significant change in the chemical part of the observed isomer shift and thus no appreciable change in the electronic structure of the iron atom. The same argument derives from the quadrupole splitting data. The lack of a pronounced temperature dependence of the quadrupole splitting indicates that the energy gap between the d_{xy} orbital and the orbital doubled (d_{xz}, d_{yz}) is much larger than the thermal energy. The two quadrupole doublets are the result of two slightly different electric field gradients because of the disorder in the oxygen sites.

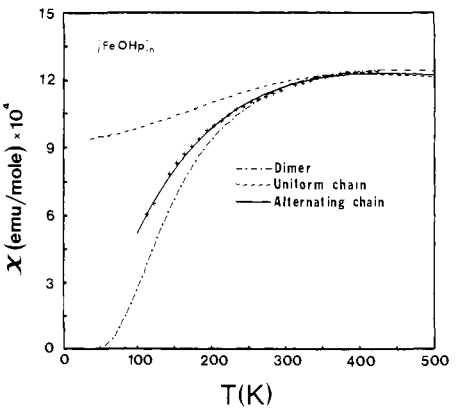

Figure 4. Magnetic susceptibility data for $[FeOHp]_n$. The full line was calculated from a scaled alternating-chain model ($S = 1$) with the best-fit parameters given in the text. The failure of the uniform-chain model and the dimer model to fit the experimental data in best-fit calculations is apparent.

Magnetic Properties. As shown in Figure 4 the magnetic susceptibility of $[FeOHp]_n$ decreases from 1.24×10^{-3} at 423 K and approaches 6×10^{-4} at 110 K, the low-temperature limit of the data collected at Tübingen. These data are in good agreement with a second set of data collected in Mainz. This second data set, which was collected in the temperature range 3.35–294.8 K, revealed a minimum in the magnetic susceptibility near 65 K. Below that temperature the magnetic susceptibility increases with the decrease in temperature. The first attempt for the analysis of these data was based on the structural information, with the assumption that the increase in magnetic susceptibility at low temperatures arose from paramagnetic impurities, defects, and finite chain-length effects and that the higher temperature data reflected antiferromagnetic exchange coupling in the linear chain.

The low-temperature data were fit to a Curie–Weiss law, $\chi = C/(T - \Theta)$, using a Simplex nonlinear least-squares fitting routine,

Table III. Bond Lengths (Å) and Angles (deg) for $[FeOHp]_n$[a]

Bond Lengths

Fe-N1	2.135 (3)	N2-C6	1.282 (4)	C6-C7	1.482 (5)
Fe-N3	1.910 (3)	N3-C6	1.379 (4)	C7-C8	1.380 (5)
Fe-O_a	2.03 (3)	N3-C9	1.377 (4)	C8-C9	1.467 (5)
Fe-O_a'	2.02 (3)	N4-C9	1.284 (4)	C7-C10	1.377 (5)
Fe-O_b	2.02 (3)	N4-C1	1.384 (4)	C10-C11	1.390 (5)
Fe-O_b'	1.97 (3)	C1-C2	1.392 (5)	C11-C12	1.385 (5)
N1-C1	1.364 (4)	C2-C3	1.371 (5)	C12-C13	1.389 (5)
N1-C5	1.356 (4)	C3-C4	1.371 (5)	C13-C8	1.387 (5)
N2-C5	1.388 (4)	C4-C5	1.388 (5)		

Bond Angles

N1-Fe-N1'	175.1 (2)	C3-C4-C5	119.2 (4)
N1-Fe-N3	90.2 (1)	N1-C5-N2	122.7 (4)
N1-Fe-N3'	89.9 (1)	N1-C5-C4	121.8 (4)
N3-Fe-N3'	175.2 (3)	N2-C5-C4	115.4 (3)
N3-Fe-N1'	89.9 (1)	N2-C6-N3	128.9 (4)
Fe-O_a-Fe	158.2 (7)	N2-C6-C7	122.4 (4)
Fe-O_b-Fe	170.5 (7)	N3-C6-C7	108.8 (4)
Fe-N1-C1	119.5 (2)	C6-C7-C8	106.3 (4)
Fe-N1-C5	119.1 (2)	C6-C7-C10	132.0 (4)
C1-N1-C5	117.6 (3)	C8-C7-C10	121.7 (4)
Fe-N3-C6	123.9 (2)	C7-C8-C9	107.5 (4)
Fe-N3-C9	123.7 (2)	C7-C8-C13	121.6 (4)
C6-N3-C9	108.5 (3)	C9-C8-C13	130.9 (4)
C5-N2-C6	123.7 (3)	N3-C9-N4	128.5 (4)
C9-N4-C1'	123.8 (4)	N3-C9-C8	108.8 (3)
N1-C1-N4'	122.3 (4)	N4-C9-C8	122.6 (4)
N1-C1-C2	121.9 (4)	C7-C10-C11	117.0 (4)
N4'-C1-C2	115.6 (4)	C10-C11-C12	121.6 (4)
C1-C2-C3	119.0 (4)	C11-C12-C13	121.1 (4)
C2-C3-C4	119.8 (4)	C12-C13-C8	117.0 (4)

O-Fe-O Angles of Type I

O_a-Fe-O_a''	158 (1)
O_a-Fe-O_b''	168 (1)
O_b-Fe-O_b''	171 (1)

O-Fe-O Angles of Type II

O_a-Fe-O_a'	180 (1)
O_b-Fe-O_a'	168 (1)
O_b-Fe-O_b'	180 (1)

[a] Standard deviations are in parentheses.

Table IV. Mossbauer Parameters (Chemical Isomer Shift δ Relative to Metallic Iron and Electric Quadrupole Splitting ΔE_Q) for the Two Iron Sites I and II as a Function of Temperature

	δ, mm s^{-1}		ΔE_Q	
T, K	site I	site II	site I	site II
4.2	0.38 (1)	0.34 (1)	1.42 (1)	1.72 (1)
294	0.28 (1)	0.22 (1)	1.46 (2)	1.64 (1)
420	0.09 (1)	0.07 (2)	1.34 (2)	1.60 (5)

with the criterion of best fit being the minimum value of the function

$$F = \sum_i w_i(\chi_i^{obsd} - \chi_i^{calcd})^2$$

with the weights being assigned $w_i = (\chi_i^{obsd})^{-1}$. The data in the temperature range 18.3–63.1 K, when corrected for the residual paramagnetism of the exchange-coupled predominant component of the sample, may be fit precisely with the Curie–Weiss parameters $C = 0.06$ and $\Theta = -25$ K. There is a sharp departure of the data at 12.8 K and lower temperatures from this Curie–Weiss law, and the lower temperature data may be fit with the parameters $C = 0.017$ and $\Theta = 4$ K. The data in the temperature range 18.3–63.1 K are thought to arise largely from a small amount of paramagnetic species, which may be a combination of defects, end effects from finite chains, and impurities. These are estimated below to be on the order of 0.4%. Conjectures concerning the strong divergent behavior of the data at 12.8 K and lower temperatures are given below.

It was anticipated that the magnetic susceptibility data above 65 K, corrected for the residual Curie susceptibility of the assumed impurity, could be accounted for in terms of Heisenberg exchange of $S = 1$ ions within a linear chain, according to the Hamiltonian

$$H = -2J\sum_{i\neq j} \hat{S}_i \cdot \hat{S}_j$$

If, as we will show below, the iron ion is in formal oxidation state +IV, then a reasonable electronic configuration is $(d_{xy})^2(d_{xz}, d_{yz})^2$. This electronic configuration yields a singly (orbitally) degenerate, single-ion ground state, and frequently exchange between ions with such ground states is isotropic if zero-field splitting effects are not large.

Table V. Coefficients for Magnetic Susceptibility Expressions for Heisenberg Chains with $S = {}^1/_2$, 1, ${}^3/_2$, 2, ${}^5/_2$, and 3

S	A	B	C	D
${}^1/_2$	0.2500	0.18297	1.5467	3.4443
1	0.6667	2.5823	3.6035	39.558
${}^3/_2$	1.2500	17.041	6.7360	238.47
2	2.0000	71.938	10.482	955.56
${}^5/_2$	2.9167	208.04	15.543	2707.2
3	4.0000	595.00	20.811	7586.7

Although there are no closed-form solutions for the magnetic susceptibility of antiferromagnetically coupled $S = 1$ chains, Weng[15] has extended work of Bonner and Fisher[16] and Fisher[17] and has given numerical results for exchange-coupled chains of $S = 1, {}^3/_2, 2, {}^5/_2$, and 3 ions. Following the lead provided by Hall[18] for Heisenberg exchange in $S = {}^1/_2$ ions and by Kahn and co-workers[19] for $S = 1$ ions, we have fit the function in eq 1 where

$$\chi_M = (Ng^2\mu_B^2/kT)[A + Bx^2][1 + Cx + Dx^3]^{-1} \quad (1)$$

$x = |J|/kT$, to Weng's numerical results and have generated the coefficients for chains with spins $S = {}^1/_2$, 1, ${}^3/_2$, 2, ${}^5/_2$, and 3. These coefficients are given in Table V to five significant figures since these were the number of digits required to obtain precise fits. The equation for the analysis of magnetic susceptibility data of chains of $S = {}^1/_2$ ions exhibiting antiferromagnetic Heisenberg exchange has been used extensively,[20] and Kahn and co-workers[19] have been successful with the use of their equation for $S = 1$. Our equation is cast in a different form from that used by Kahn and co-workers[19] and, as a result, the two sets of coefficients differ. The magnetic susceptibility data above 110 K cannot be fit with any of the linear-chain equations for any spin value with any values for the exchange coupling constant J and electron g value; see Figure 4.

As shown in Figure 4, the complete set of magnetic susceptibility data for $[FeOHp]_n$ above 110 K also cannot be fit satisfactorily with theory for antiferromagnetically exchange-coupled pairs of $S = 1$ ions. The best fit of the data to the equation for pairwise exchange between $S = 1$ ions is obtained with the parameters $J = -150$ cm^{-1} and $g = 2.34$. Comparable equations for isotropic exchange coupling between pairs of ions with spin values of $S = {}^3/_2$, 2, and ${}^5/_2$ ions gave equally unsatisfactory results.

As discussed below, there remained the possibility that the compound had iron in formal oxidation state +III, with the hemiporphyrazine ligand being a radical anion, and that these were exchange coupled. This possibility was ruled out by the failure of equations for exchange coupling between an $S = {}^1/_2$ ion and $S = {}^3/_2$ or $S = {}^5/_2$ ion to fit the magnetic susceptibility data. There are presently no available models for the magnetic behavior of a uniform Heisenberg chain which has every ion in the chain interacting with an $S = {}^1/_2$ ion exterior to the chain.

(15) Weng, C. H. Ph.D. Dissertation, Carnegie-Mellon University, Pittsburgh, PA, 1968.
(16) Bonner, J. C.; Fisher, M. E. *Phys. Rev., Sect. A* **1964**, *135*, 640.
(17) (a) Fisher, M. E. *Am. J. Phys.* **1964**, *32*, 343. (b) Fisher, M. E. *J. Math. Phys.* **1963**, *4*, 124–135.
(18) Hall, J. W. Ph.D. Dissertation, The University of North Carolina at Chapel Hill, Chapel Hill, NC, 1977.
(19) Meyer, A.; Gleizes, A.; Girerd, J.-J.; Verdaguer, M.; Kahn, O. *Inorg. Chem.* **1982**, *21*, 1729–1739.
(20) Hatfield, W. E.; Weller, R. R.; Hall, J. W. *Inorg. Chem.* **1980**, *19*, 3825–3828.

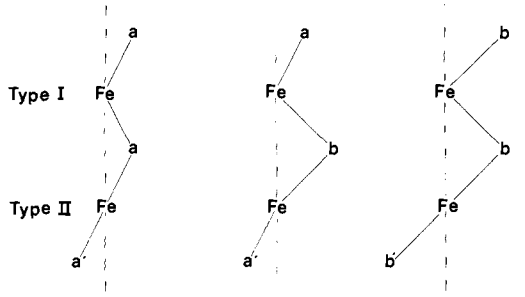

Figure 5. Schematic drawing of the chain illustrating the disorder in the oxygen sites.

The absence of an EPR resonance could signal a large zero-field splitting, and, in such cases, anisotropic exchange is common. We attempted to fit scaled versions of the following equations for Ising exchange, i.e., $H_{ex} = -2J\sum_{i\neq j}\hat{S}_i^z\hat{S}_j^z$, to the magnetic susceptibility data:

$$\chi_{\parallel} = (Ng^2\mu_B{}^2/4k_BT)[\exp(-2|J|/k_BT)]$$

$$\chi_{\perp} = (Ng^2\mu_B{}^2/8|J|)[\tanh(|J|/k_BT) + (|J|/k_BT)\,\mathrm{sech}^2(|J|/k_BT)]$$

The average susceptibility was calculated from $\chi_{av} = (1/3)(\chi_{\parallel} + 2\chi_{\perp})$. The scaled Ising equations failed to fit the experimental data.

Since the bridging oxygens are randomly distributed in four possible positions, it seemed likely that theory for random exchange might be successful in accounting for the magnetic susceptibility data. Scott et al.[21] have modified Fisher's solution for the magnetic susceptibility of a chain of classical spins ($S = \infty$)[17] and have developed the following expression for a chain in which the exchange coupling constant varies randomly with the bridge:

$$\chi_M = [Ng^2\mu_B{}^2S(S+1)/3kT][(1-\langle u\rangle)/(1+\langle u\rangle)]$$

where

$$\langle u\rangle = (-kT/2JS\{S+1\})\ln\{(2J+\lambda)\sinh[(2J-\lambda)S(S+1)/kT]((2J-\lambda)\sinh[(2J+\lambda)S(S+1)/kT])^{-1}\}$$

This expression does not fit the experimental data with any reasonable values of J, g, and λ for which it is valid. But this is not surprising since there are only two distinct oxygen bridges (and therefore only two exchange pathways corresponding to two exchange coupling constants) and not some thermally populated or averaged range of positions that could potentially lead to a distribution (i.e., randomly disposed about a mean value) of exchange constants.

As shown in Figure 4, the magnetic susceptibility data can be described by a scaled theoretical expression for exchange coupling in an alternating chain of $S = 1$ ions[22] with $J = -133$ cm^{-1}, $g = 2.30$, and the alternation parameter $\alpha = 0.4$. The data are shown down to 100 K since below $kT/J = 0.5$ the theoretical results are not reliable. The parameters are defined by the Hamiltonian

$$H = -2J\sum_{i=1}^{n/2}[\hat{S}_{2i}\cdot\hat{S}_{2i-1} + \alpha\hat{S}_{2i}\cdot\hat{S}_{2i+1}]$$

where J is the exchange integral between a spin and its right neighbor and αJ is the exchange integral between a spin and its left neighbor. The use of an alternating chain was suggested by the disorder in the oxygen position, which yields two different Fe–O–Fe bridging networks in the chain. Therefore, there are only two values for the exchange coupling constant, and not a distribution of J values as implied by the random exchange model. The alternating-chain model is discussed more fully in the Discussion section.

(21) Scott, J. C.; Garito, A. F.; Heeger, A. J.; Nannelli, P.; Gillman, H. D. *Phys. Rev. B: Solid State* **1975**, *12*, 356–361.
(22) ter Haar, L. W.; Hatfield, W. E., unpublished observations.

Discussion

Structure of [FeOHp]$_n$. Even with the severe distortion of the hemiporphyrazine system, the central iron atom and the four donor atoms N1, N3, N1′, and N3′ form a planar configuration; the Fe–N distances of 1.910 and 2.135 Å are significantly different, and the shorter distances are those to the nitrogen atom of the isoindole units. This observation suggests that the basicity of the nitrogen atom N3 is enhanced by an interruption of the conjugation in the internal C(6–9)–N(3) ring. This conclusion is further supported by the bond distances C6–N2 and C9–N4, which are consistent with localized double bonds. C6–N2 and C9–N4 involve carbon atoms of the isoindole unit. The origin of the interference with the conjugation is the more stable electronic structure associated with intact 6π systems of the pyridine rings and the six-membered rings B. Similar bonding relationships were found in [HpGe{C≡CC(CH$_3$)$_3$}$_2$], where the Ge–N distances are 1.956 and 2.172 Å.[14]

The saddle shape of the metallomacrocycle is reminiscent of the same shape adopted by complexes of sterically hindered dibenzotetraaza[14]annulene ligands.[23] The dibenzotetraaza[14]annulene can be modified, with the exocyclic steric hindrance being removed, and strictly planar complexes are formed with first-row[24] and second-row[25] transition series metal ions. Since there is no exocyclic steric hindrance on the hemiporphyrazine ligand, the saddle shape may arise from the small size and irregular shape of the four-coordinate hole of the macrocyclic ligand relative to the size of the iron ion. Alternatively, there may be some special stability associated with an interaction between the axial oxygen ions and the π-clouds of the six-membered rings. Additional experimental work under way on other complexes of hemiporphyrazines may yield additional information on the origin of this structural feature.

Oxidation State and Electronic Configuration of Iron. Formal oxidation states of +IV or +III can be assigned for the iron ion, but in the latter case, which corresponds to Hp^{1-}Fe^{3+}O^{2-}, the hemiporphyrazine ring would be a radical anion. Many such radical anions exhibit intense EPR signals in the area of the free-electron g value.[26] No EPR absorptions were observed on a polycrystalline sample of [FeOHp]$_n$ at several different temperatures (292, 113, and 80 K). This experimental observation, coupled with the failure of exchange models for an $S = {}^1/_2$ ligand radical and an $S = {}^3/_2$ or $S = {}^5/_2$ metal ion to account for the magnetic susceptibility data, is strong supporting evidence for the +IV formal oxidation state, indicated by the formula [FeOHp]. In addition, it is well-known that it is difficult to detect EPR spectra in systems with even spin,[27] an additional observation that supports the oxidation state of +IV and spin state $S = 1$.

In planar macrocyclic complexes, only the d_{xz} and d_{yz} orbitals of the metal are capable of π-bonding, and in fourfold symmetry these two orbitals transform as e. This degeneracy is lifted in the present case, but for the purposes of this discussion, it is sufficient to note that the energies of these two orbitals will be essentially the same. The $d_{x^2-y^2}$ orbital is strongly σ-antibonding, the d_{z^2} orbital is weakly σ-antibonding, and the d_{xy} orbital is essentially nonbonding. This results in the following orbital splitting pattern:

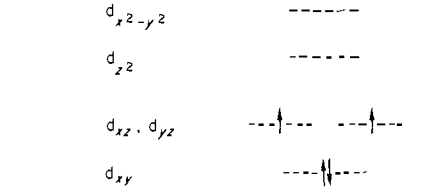

(23) Goedken, V. L.; Peng, S. M.; Norris, J. M.; Park, Y.-A. *J. Am. Chem. Soc.* **1976**, *98*, 8391 and references therein.
(24) Weiss, M. C.; Gordon, G.; Goedken, V. L. *Inorg. Chem.* **1977**, *16*, 305.
(25) Hatfield, W. E. *Polym. Sci. Technol.* **1981**, *15*, 57–69.
(26) Myers, J. F.; Canham, G. W. R.; Lever, A. B. P. *Inorg. Chem.* **1975**, *14*, 461.
(27) Palmer, G. In "Iron Porphyrins, Part II"; Lever, A. B. P., Gray, H. B., Eds.; Addison-Wesley: Reading, MA, 1983; Chapter 2.

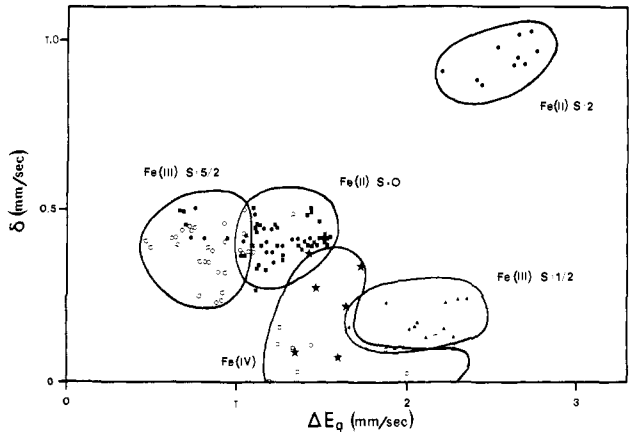

Figure 6. Isomer shifts δ and quadrupole splittings ΔE_Q for several iron porphyrin compounds with oxidation states +II and +III. The Mössbauer data for $[FeOHp]_n$ are indicated by stars. The isomer shifts are relative to metallic iron as a standard, and data are given for various temperatures. See ref 33.

Evidence for this array and spin state is provided by the Mössbauer spectra. The weak temperature dependence of ΔE_Q is consistent with a spin-Hamiltonian formalism using $S = 1$ for an iron(IV) system.[28] The Mössbauer parameters in Table IV are also in agreement with the tabulated data for other iron(IV) systems.[31-33]

In Figure 6 we have collected isomer shift and quadrupole splitting data for a number of iron porphyrin compounds with a range of oxidation states and spin multiplicities. We will now show that the Mössbauer data and/or the magnetic susceptibility data are consistent only with an oxidation state of +IV for iron. The Mössbauer data in Figure 6 for high-spin ($S = 2$) iron(II) differ remarkably from those of $[FeOHp]_n$, and since the compound is paramagnetic with a magnetic moment of 2.05 μ_B at 423 K, low-spin ($S = 0$) iron(II) can be eliminated as a possibility. The magnetic and Mössbauer data eliminate $S = 0$ and $S = 2$ spin states and oxidation state +II for iron in $[FeOHp]_n$.

The Mössbauer data in Figure 6 for high-spin ($S = {}^5/_2$) iron(III) are substantially different from those of $[FeOHp]_n$, and this spin and oxidation state can be eliminated as a possibility. The most convincing evidence for the elimination of low-spin ($S = {}^1/_2$) iron(III) as a possibility is provided by the magnetic data. A magnetic moment of 2.05 μ_B is much too large for a strongly exchange-coupled $S = {}^1/_2$ system. If we conclude from the data in Figure 4 that the magnetic susceptibility has reached its maximum value near 400 K, then a g value greater than 3 is required for an exchange-coupled pair of $S = {}^1/_2$ ions to exhibit a magnetic moment of 2.05 μ_B at 400 K. A g value greater than 4 is required for a chain of exchange-coupled $S = {}^1/_2$ ions to exhibit the same moment. These g values are much too large to be realistic, and the low-spin ($S = {}^1/_2$) iron(III) possibility for $[FeOHp]_n$ can be eliminated.

As shown in Figure 6, the Mössbauer data for $[FeOHp]_n$ are similar to those reported for other iron(IV) compounds with established or proposed $S = 1$ spin states.

Exchange Coupling in $[FeOHp]_n$. The magnetic susceptibility data for $[FeOHp]_n$ may be described by an alternating-chain model. The applicability of the model may be understood in terms of the structure and disorder in the oxygen positions. As shown schematically in Figure 5, all [FeHp] moieties are translationally equivalent; however, the details of the iron site are dictated by the occupancy of the oxygen sites, which are labeled a, a', b, and b' in Figure 5. A type I iron site has oxygen neighbors arranged in a syn fashion, while a type II iron site has oxygen neighbors arranged in an anti fashion. As shown in Figure 5, a type I site can arise from adjacent oxygen occupancy in sites (a, a), (b, b), and (a, b), while a type II site arises from adjacent oxygen occupancy in sites (a, a'), (b, b'), or (b, a'). Since the Mössbauer spectra provide evidence for only two iron sites, we conclude that the experiment is not sensitive enough to the three kinds of type I and type II sites to reflect their presence in the spectrum.

It has been well established that subtle changes in the superexchange pathway may have large effects on the exchange coupling constant,[29] and the exchange coupling constant correlates well with the structural features of the bridge, specifically with the quotient ϕ/r_0 where ϕ is the angle at the bridge and r_0 is the bond distance. Since the ϕ/r_0 values for the two bridges are 78.1 and 85.4, it may be expected that pairwise exchange in Fe–O_a–Fe differs from that in Fe–O_b–Fe (where the subscripts designate the site of the bridging oxygen) but that both are expected to have relatively large negative exchange coupling constants. The alternation parameter of 0.4, which resulted from the analysis of the magnetic susceptibility data, provides experimental documentation for this conclusion.

The magnetic susceptibility behavior, the Mössbauer spectra, and the X-ray structural results are consistent with a chain structure for $[FeOHp]_n$ in which the bridging oxygens are randomly distributed among four positions, yielding an infinite chain containing two different spin-exchange bridging networks for superexchange interactions and two different types of iron sites. Short sections of this infinite chain could probably be uniform chainlike segments containing only type a or type b oxygen bridges. However, the magnetic susceptibility data indicate, and it would be reasonable to expect on a statistical basis, that the predominate nature of the short segments would be alternating type a and type b oxygen bridges. Theoretical calculations[30] on small clusters of alternating $S = {}^1/_2$ ions have shown that the magnetic susceptibilities below χ_{max} of antiferromagnetically exchange-coupled short chains have substantially the same variation with temperature. It is not possible to determine a distribution of segment lengths from bulk magnetic susceptibility data.

There is a strong divergence of the magnetic susceptibility at the lowest temperatures. This may be understood in terms of a model in which there is random exchange between the "odd" iron ion, i.e., Fe_3, in a segment such as

$$\cdots Fe_1\text{–}O_s\text{–}Fe_2\text{–}O_w\text{–}Fe_3\text{–}O_w\text{–}Fe_4\text{–}O_s\text{–}Fe_5\text{–}O\cdots$$

with similar ions in nearby segments. Here the subscripts s and w on the bridging oxygen designate stronger and weaker pairwise exchange coupling, respectively. Extensive magnetization studies and heat capacity studies at low temperatures will be necessary to verify this suggestion.

Fe–O–Fe Bridging Angle. The presence of the bridging oxygen in two different crystallographic sites leads to two Fe–O–Fe bridging angles. The question of the features that control the bridging angle in μ-oxo-bridged iron compounds continues to attract attention.[34,35] Data exist for a number of μ-oxo-bridged iron(III) compounds, and features such as ligand repulsions, electronic effects, and crystal packing have been invoked to explain the usual nonlinearity of the Fe–O–Fe linkage.

The data for $[FeOHp]_n$ have a significant bearing on the question of the Fe–O–Fe angle. Ligand repulsions are identical and in-plane electronic effects are identical, and yet the two angles differ by about 12°, being 158.2 (7)° in one case and 170.5 (7)° in the other. An examination of the structural data does not reveal significant differences in the oxygen sites, and crystal packing is unlikely to be important. Since the magnetic data suggest a regular alternation, it would appear that there is a significant out-of-plane trans effect. Experiments designed to yield infor-

(28) Münck, E. In "The Porphyrins"; Dolpin, D., Ed.; Academic Press: New York, 1979; Vol. IV, Chapter 7.
(29) Hatfield, W. E. *Comments Inorg. Chem.* **1981**, *1*, 105–121.
(30) Weller, R. R. Ph.D. Dissertation, The University of North Carolina at Chapel Hill, Chapel Hill, NC, 1980.
(31) English, D. R.; Hendrickson, D. N.; Suslick, K. S. *Inorg. Chem.* **1983**, *22*, 367–368.
(32) Maeda, Y. *J. Phys., Coll. C2, Suppl. No. 3* **1979**, *40*, C2:514–C2:522.
(33) Sams, J. R.; Tsin, T. B. In "The Porphyrins"; Dolphin, D., Ed.; Academic Press: New York, 1979; Vol. IV, Chapter 9.
(34) Murray, K. S. *Coord. Chem. Rev.* **1974**, *12*, 1–35.
(35) Landrum, J. T.; Grimmitt, D.; Haller, K. J.; Scheidt, W. R.; Reed, C. A. *J. Am. Chem. Soc.* **1981**, *103*, 2640–2650.

mation concerning this out-of-plane trans effect are under way with analogous compounds.

Acknowledgment. We thank J. Ensling, C. P. Köhler, and K. Römhild for experimental assistance. This research was supported in part by the Deutsche Forschungsgemeinschaft, the Stiftung Volkswagenwerk, the Fonds der Chemischen Industrie, the Office of Naval Research, and the National Science Foundation.

Registry No. $[FeOHp]_n$, 87901-24-4.

Supplementary Material Available: Table of observed and calculated structure factors for $[FeOHp]_n$ (15 pages). Ordering information is given on any current masthead page.

Configurational Stability of the 2,2-Diphenyl-1-(trimethylsilyl)cyclopropyl Carbanion and Free Radical. Absolute Stereochemical Assignments to Select Silylcyclopropanes[1]

Leo A. Paquette,* Takane Uchida,[2a] and Judith C. Gallucci[2b]

Contribution from the Evans Chemical Laboratories, The Ohio State University, Columbus, Ohio 43210. *Received June 27, 1983*

Abstract: 2,2-Diphenylcyclopropanecarboxylic acid was silylated at the 1-position and this product was resolved with *l*-cinchonidine. The resulting optically active acid was transformed into (−)-2,2-diphenyl-1-methyl-1-(trimethylsilyl)cyclopropane, whose absolute configuration was shown to be *R* by metalation and silylation of (−)-(*R*)-**6**. The latter reaction proceeds with retention of configuration. In this way, the levorotatory form of (−)-**3** was established to be *R*. Whereas the Hunsdiecker degradation of (−)-(*R*)-**3** produced only racemic bromide, application of the Haller–Bauer process to (+)-(*R*)-phenyl ketone **12** led to (−)-(*R*)-silane **13**. That this carbanion-mediated reaction proceeded with complete retention of stereochemistry was confirmed by preparation of (+)-1-(*S*)-3-(*S*)-**16** and X-ray analysis of its *l*-menthyl ester (**17**), in tandem with suitable transformation of (−)-1-(*R*)-3-(*R*)-**16** to the identical levorotatory silane **13**. The failure of the α-silyl cyclopropyl free radical to maintain configuration and the nonracemizability of its carbanion counterpart are discussed in the light of silicon's capacity for stabilizing neighboring reactive centers.

Although α-silyl carbanions are gaining increased importance in synthesis,[3] the manner in which silicon stabilizes adjacent carbon–metal bonds remains unclear. The electron-attracting capability of R_3Si substituents, which overrides the greater electropositive character of silicon relative to carbon, has been recognized for many years.[4] Early rationalizations of this stabilizing influence favored a d_π-p_π model (A) wherein overlap of

A B C

an empty d orbital on Si having the proper symmetry with the filled carbanion orbital leads to a decrease in energy. Although such thinking remains popular,[5] an alternative explanation has been advanced which discounts the importance of d orbitals. According to the latter argument, an empty σ* orbital on Si can

Scheme I

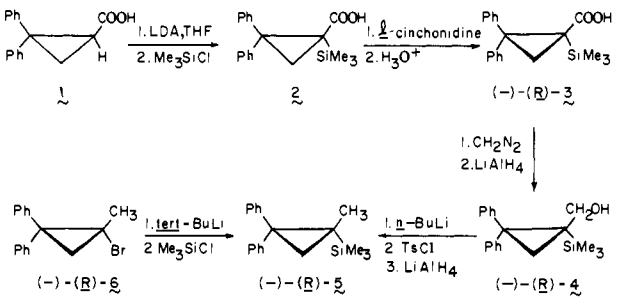

overlap adequately well with the filled orbital of a covalent carbon-metal bond (B) to account for the stabilization.[6,7] The importance of n_C-σ^*_{SR} charge-transfer interactions to α-thia carbanions has been studied in depth by perturbation MO methods,[8] and it may well be that polarization of the C–Si bond in the $C^{\delta-}$–$Si^{\delta+}$ direction is adequate to guarantee the level of stabilization encountered.

(1) Silanes in Organic Synthesis. 21. For part 20, see: Paquette, L. A.; Charumilind, P.; Galucci, J. C. *J. Am. Chem. Soc.* **1983**, *105*, 7364.

(2) (a) Postdoctoral Researcher on sabbatical leave from Fukui University, Bunkyo, Fukui 910, Japan. (b) Author to whom inquiries concerning the X-ray crystal structure analysis should be directed.

(3) Magnus, P. *Aldrichchimica Acta* **1980**, *13*, 43.

(4) For some early examples, consult: (a) Eaborn, C. "Organosilicon Compounds"; Butterworths: London, 1960. (b) Bazant, V.; Chvalovsky, V.; Rathousky, J. "Organosilicon Compounds"; Academic Press: New York, 1965; Vol. 1. (c) Bott, R. W.; Eaborn, C. In "Organometallic Compounds of the Group IV Elements"; MacDiarmid, A. G., Ed.; Marcel Dekker: New York, 1968; Vol. 1, Part 1, Chapter 2.

(5) Kwart, H.; King, H. G. "d-Orbitals in the Chemistry of Silicon, Phosphorus, and Sulfur"; Springer-Verlag: New York, 1977.

(6) (a) Pitt, C. G. *J. Organometal. Chem.* **1973**, *61*, 49. (b) Ensslin, W.; Bock, H.; Becker, G. *J. Am. Chem. Soc.* **1974**, *96*, 2757. (c) Jung, I. N.; Jones, P. R. *J. Organometal. Chem.* **1975**, *101*, 27, 35. (d) Ponec, R.; Chernyshev, E. A.; Tolstikova, N. G.; Chvalovsky, V. *Collect. Czech. Chem. Commun.* **1976**, *41*, 2714. (e) Reynolds, W. F.; Hamer, G. K.; Bassindale, A. R. *J. Chem. Soc., Perkin Trans. 2* **1977**, 971. (f) Ramsey, B. G. *J. Organometal. Chem.* **1977**, *135*, 307. (g) Adcock, W.; Aldous, G. L.; Kitching, W. *Tetrahedron Lett.* **1978**, 3387.

(7) (a) Fleming, I. In "Comprehensive Organic Chemistry"; Barton, D. H. R., Ollis, W. D., Eds.; Pergamon Press: Oxford, 1979; Vol. 3, Chapter 13. (b) Colvin, E. W. "Silicon in Organic Synthesis"; Butterworths: London, 1981.

(8) (a) Epiotis, N. D.; Yates, R. L.; Bernardi, F.; Wolfe, S. *J. Am. Chem. Soc.* **1976**, *98*, 5435. (b) Lehn, J.-M.; Wipff, G. *Ibid.* **1976**, *98*, 7498.

0002-7863/84/1506-0335$01.50/0